Supplementary material: Richtmyer–Meshkov instability when a shock is reflected for fluids with arbitrary equation of state

M. Napieralski, F. Cobos, A.L. Velikovich, and C. Huete

S.1. Base-flow quilibrium conditions

To calculate the base flow equilibrium, it is necessary to solve the conservation equations across the shocks along with the mechanical equilibrium condition at the interface. In the absence of disturbances, the regions separated by each shock wave and the contact interface are steady and uniform. The changes in flow variables across each shock are governed by the Rankine-Hugoniot (RH) equations, which state:

$$[\rho u] = 0, \quad \left[p + \rho u^2\right] = 0, \quad \left[E + \frac{p}{\rho} + \frac{1}{2}u^2\right] = 0, \tag{S.1.1}$$

for mass, momentum, and energy, respectively, where the square brackets $[\ldots]$ denote the difference between the indicated quantities' values ahead and behind the shock front. In (S.1.1), ρ, u, p, and E represent density, velocity, pressure, and internal energy, respectively, evaluated on both sides of each shock wave. The material velocity is measured in the corresponding shock reference frame. The zero-order problem formulation is completed after providing the equilibrium conditions that must be imposed at the planar interface: $p_{2t} = p_{2r}$ and $U_2(x < 0) = U_2(x > 0)$. The notation used here corresponds to the sketch in Fig. 1 of the main text. Additionally, along with the isobaric condition, an extra parameter is required to relate the initial thermodynamic states of the fluids on both sides of the interface. The parameter typically used is the pre-interaction Atwood number, defined as

$$\mathcal{A}_0 = \frac{\rho_{0t} - \rho_{0r}}{\rho_{0t} + \rho_{0r}} \tag{S.1.2}$$

that is bounded by $-1 < \mathcal{A}_0 < 1$. The pressure continuity at the contact interface, $p_{2t} = p_{2r}$, can be written as a function of the shock pressure jumps:

$$\mathcal{P}_r \mathcal{P}_i = \mathcal{P}_t, \tag{S.1.3}$$

where $\mathcal{P}_r = p_{2r}/p_{1r}$, $\mathcal{P}_i = p_{1r}/p_{0r}$, and $\mathcal{P}_t = p_{2t}/p_{0t}$ correspond to the pressure jump functions across the reflected, incident and transmitted shocks, respectively. On the other hand, the continuity in the streamwise velocity $U_2(x < 0) = U_2(x > 0)$ renders

$$\mathcal{M}_i(1 - \mathcal{R}_i^{-1}) - \mathcal{M}_r(1 - \mathcal{R}_r^{-1})\sqrt{\frac{\kappa_{1r}}{\kappa_r}\frac{\mathcal{P}_i}{\mathcal{R}_i}} = \mathcal{M}_t(1 - \mathcal{R}_t^{-1})\sqrt{\frac{\kappa_t}{\kappa_r}\frac{1 - \mathcal{A}_0}{1 + \mathcal{A}_0}} \tag{S.1.4}$$

that involves more parameters. The functions $\mathcal{M}_r = (D_R + U_1)/c_{1r}$, $\mathcal{M}_i = D_I/c_{0r}$, and $\mathcal{M}_t = D_T/c_{0t}$ stand for the reflected, incident and transmitted shock Mach numbers, respectively. The c functions identify the corresponding sound speeds, that must be computed upon determination of the associated EoS. Equation (S.1.4) also depends on the corresponding density jump functions, which read, $\mathcal{R}_r = \rho_{2r}/\rho_{1r}$, $\mathcal{R}_i = \rho_{1r}/\rho_{0r}$, and $\mathcal{R}_t = \rho_{2t}/\rho_{0t}$. Additionally, the associated sonic coefficients, that in the general case are state functions, are defined as $\kappa = \rho c^2/p$, where, again, c represents the speed of sound. Finally, the post shock Mach numbers are defined as $\mathcal{M}_{2r} = (D_R + U_2)/c_{2r}$, $\mathcal{M}_{2i} = (D_I - U_1)/c_{1r}$, and $\mathcal{M}_{2t} = (D_T - U_2)/c_{2t}$.

S.2. Equilibrium conditions for Van der Waals equations of state

The Van der Waals (vdW) equation of state (EoS) provides a more accurate description of real fluid behaviour than the ideal gas law. It takes into account the effect associated with non-contact interaction between particles and the finite volume they occupy. In this case, pressure and internal energy read as

$$p = \frac{\rho R_g T}{1 - b\rho} - a\rho^2 \quad \text{and} \quad E = \frac{R_g T}{\gamma - 1} - a\rho, \tag{S.2.1}$$

where R_g is the gas constant and γ is the adiabatic index. The parameters a and b have positive values and are specific to each gas. With respect to the ideal gas EoS, the term involving the constant a corrects for intermolecular attraction, while b represents the volume occupied by the gas particles. The speed of sound and the internal energy are written as functions of pressure and density

$$c^2 = \frac{\gamma(p + \rho^2 a)}{\rho(1 - b\rho)} - 2a\rho \quad \text{and} \quad E = \frac{(p + \rho^2 a)(1 - b\rho)}{\rho(\gamma - 1)} - a\rho. \tag{S.2.2}$$

It is readily seen that the (S.2.1) shifts to the ideal gas model when a and b approach zero, namely $p = \rho R_g T$ and $E = R_g T/(\gamma - 1)$. Simple manipulation of (S.2.2) provides $c^2 = \gamma R_g T = \gamma p/\rho$ as the square of the speed of sound for an ideal gas.

To compute the shock jump conditions across the shocks, the dimensionless constants are conveniently reduced with preshock conditions, *i.e.*, $\nu_r = a_r \rho_{0r}^2/p_{0r}$ and $\mu_r = b_r \rho_{0r}$, yielding the following RH curve for the incident shock:

$$\mathcal{P}_i = \frac{\mathcal{R}_i\left[\gamma_r + 1 - 2\mu_r(\nu_r + 1) - 2\nu_r(\gamma_r - 2)\right] - (\gamma_r - 1) + 2\nu_r \mathcal{R}_i^2\,(\gamma_r - 2 + \mu_r \mathcal{R}_i)}{(\gamma_r + 1) - \mathcal{R}_i\,(\gamma_r - 1 + 2\mu_r)}, \tag{S.2.3}$$

where the pressure jump $\mathcal{P}_i = p_{1r}/p_{0r}$ is expressed as function of the density jump $\mathcal{R}_i = \rho_{1r}/\rho_{0r}$ and the three parameters associated with the EoS: γ_r, ν_r and μ_r. Likewise, upon definition of $\nu_t = a_t \rho_{0t}^2/p_{0t}$ and $\mu_t = b_t \rho_{0t}$ for the transmitted shock, and $\nu_{1r} = a_r \rho_{1r}^2/p_{1r}$ and $\mu_{1r} = b_r \rho_{1r}$ for the reflected shock, the corresponding RH curves are:

$$\mathcal{P}_t = \frac{\mathcal{R}_t\left[\gamma_t + 1 - 2\mu_t(\nu_t + 1) - 2\nu_t(\gamma_t - 2)\right] - (\gamma_t - 1) + 2\nu_t \mathcal{R}_t^2\,(\gamma_t - 2 + \mu_t \mathcal{R}_t)}{(\gamma_t + 1) - \mathcal{R}_t\,(\gamma_t - 1 + 2\mu_t)}, \tag{S.2.4a}$$

$$\mathcal{P}_r = \frac{\mathcal{R}_r\left[\gamma_r + 1 - 2\mu_{1r}(\nu_{1r} + 1) - 2\nu_{1r}(\gamma_r - 2)\right] - (\gamma_r - 1) + 2\nu_{1r} \mathcal{R}_r^2\,(\gamma_r - 2 + \mu_{1r} \mathcal{R}_r)}{(\gamma_r + 1) - \mathcal{R}_r\,(\gamma_r - 1 + 2\mu_{1r})}, \tag{S.2.4b}$$

where the pressure jumps $\mathcal{P}_r = p_{2r}/p_{1r} = \mathcal{P}_r(\mathcal{R}_r, \gamma_r, \nu_r, \mu_r)$ and $\mathcal{P}_t = p_{2t}/p_{0t} = \mathcal{P}_t(\mathcal{R}_t, \gamma_t, \nu_t, \mu_t)$ are explicit functions of the density jumps ($\mathcal{R}_r = \rho_{2r}/\rho_{1r}$ and $\mathcal{R}_t = \rho_{2t}/\rho_{0t}$) and the EoS parameters. Notice that the EoS parameters for the reflected shock are in fact functions of the incident shock intensity and this relationship is explicitly established through straightforward scaling: $\nu_{1r} = \nu_r \mathcal{R}_i^2/\mathcal{P}_i$ and $\mu_{1r} = \mu_r \mathcal{R}_i$.

It is found convenient to describe the dependence of the postshock flow with the corresponding shock strengths, which can be deduced with the aid of the Rayleigh–Michelson relationships, i.e., from direct combination of mass and momentum conservation equations, the corresponding shock Mach numbers can be derived:

$$\mathcal{M}_i^2 = \frac{\mathcal{P}_i - 1}{1 - \mathcal{R}_i^{-1}} \frac{1}{\kappa_r}, \qquad \mathcal{M}_t^2 = \frac{\mathcal{P}_t - 1}{1 - \mathcal{R}_t^{-1}} \frac{1}{\kappa_t}, \qquad \mathcal{M}_r^2 = \frac{\mathcal{P}_r - 1}{1 - \mathcal{R}_r^{-1}} \frac{1}{\kappa_{1r}}, \tag{S.2.5}$$

for the incident, transmitted and reflected shocks, respectively. In writing (S.2.5), we have made use of the sonic coefficient $\kappa = \rho c^2/p$ that takes the following form for each shock wave:

$$\kappa_r = \gamma_r \frac{1+\nu_r}{1-\mu_r} - 2\nu_r, \quad \kappa_t = \gamma_t \frac{1+\nu_t}{1-\mu_t} - 2\nu_t, \quad \kappa_{1r} = \gamma_r \frac{1+\nu_{1r}}{1-\mu_{1r}} - 2\nu_{1r}. \tag{S.2.6}$$

Likewise, the postshock Mach numbers are explicit functions of the previous relationships:

$$\mathcal{M}_{2i}^2 = \frac{\mathcal{M}_i^2}{\mathcal{R}_i \mathcal{P}_i} \frac{\kappa_r}{\kappa_{1r}}, \qquad \mathcal{M}_{2t}^2 = \frac{\mathcal{M}_t^2}{\mathcal{R}_t \mathcal{P}_t} \frac{\kappa_t}{\kappa_{2t}}, \qquad \mathcal{M}_{2r}^2 = \frac{\mathcal{M}_r^2}{\mathcal{R}_r \mathcal{P}_r} \frac{\kappa_{1r}}{\kappa_{2r}} \tag{S.2.7}$$

where the post-interaction reflected and transmitted sonic coefficients are:

$$\kappa_{2r} = \gamma_r \frac{1+\nu_{1r}\mathcal{R}_r^2/\mathcal{P}_r}{1-\mu_{1r}\mathcal{R}_r} - 2\nu_{1r}\mathcal{R}_r^2/\mathcal{P}_r, \quad \kappa_{2t} = \gamma_t \frac{1+\nu_t\mathcal{R}_t^2/\mathcal{P}_t}{1-\mu_t\mathcal{R}_t} - 2\nu_t\mathcal{R}_t^2/\mathcal{P}_t. \tag{S.2.8}$$

Beyond the postshock Mach numbers ($\mathcal{M}_{2r}$, $\mathcal{M}_{2t}$), and density jumps ($\mathcal{R}_r$, $\mathcal{R}_t$), the linear problem demands the knowledge of additional parameters for each transmitted and reflected shocks. They are the corresponding shock ripple initial amplitudes ξ_t^0 and ξ_r^0, and the so-called DK parameters, h_t and h_r that measures the slope of the RH curve in the post-shock state. The latter are simply given by

$$h_t = -\kappa_t \frac{\mathcal{M}_t^2}{\mathcal{R}_t^2} \left(\frac{\partial \mathcal{P}_t}{\partial \mathcal{R}_t}\right)^{-1}, \qquad h_r = -\kappa_{1r} \frac{\mathcal{M}_r^2}{\mathcal{R}_r^2} \left(\frac{\partial \mathcal{P}_r}{\partial \mathcal{R}_r}\right)^{-1}, \tag{S.2.9}$$

while the initial amplitudes take the following form

$$\xi_t^0 = 1 - \frac{D_T}{D_I} = 1 - \frac{\mathcal{M}_t}{\mathcal{M}_i}\sqrt{\frac{\kappa_t}{\kappa_r}\frac{1-\mathcal{A}_0}{1+\mathcal{A}_0}}, \quad \xi_r^0 = 1 + \frac{D_R}{D_I} = \mathcal{R}_i^{-1} + \frac{\mathcal{M}_r}{\mathcal{M}_i}\sqrt{\frac{\kappa_{1r}}{\kappa_r}\frac{\mathcal{P}_i}{\mathcal{R}_i}}. \tag{S.2.10}$$

The initial amplitude of the interface is also required to compute the transient stage of the RMI. Measured right after the two shocks detach, it differs from the pre-interaction amplitude:

$$\xi_i^0 = 1 - \frac{U_2}{D_I} = 1 - (1-\mathcal{R}_t^{-1})\frac{\mathcal{M}_t}{\mathcal{M}_i}\sqrt{\frac{\kappa_t}{\kappa_r}\frac{1-\mathcal{A}_0}{1+\mathcal{A}_0}}. \tag{S.2.11}$$

Finally, the β parameter is found useful in the linear problem formulation as it relates the speeds of sound behind the transmitted and reflected shocks. A specific relationship for two vdW gases reads as:

$$\beta = \frac{c_{2r}}{c_{2t}} = \frac{\mathcal{M}_{2t}\mathcal{R}_t\mathcal{M}_r}{\mathcal{M}_{2r}\mathcal{R}_r\mathcal{M}_t}\sqrt{\frac{\mathcal{P}_i}{\mathcal{R}_i}\frac{\kappa_{1r}}{\kappa_t}\frac{1-\mathcal{A}_0}{1+\mathcal{A}_0}} = \sqrt{\frac{\mathcal{R}_t}{\mathcal{R}_r\mathcal{R}_i}\frac{\kappa_{2r}}{\kappa_{2t}}}. \tag{S.2.12}$$

An arbitrary example of the post-interaction equilibrium is presented in Fig.S.1, where diagram pressure-velocity is computed for a shock moving with different intensities ($\mathcal{M}_i$ = 1.235, 2, 3 and 4) and the interface is characterised by the Atwood number $\mathcal{A}_0 = 2/3$ and the EoS coefficients: $\gamma_r = 31/30$, $\nu_r = 0$, $\mu_r = 0$ (highly compressible ideal gas) and $\gamma_t = 31/30$, $\nu_r = 0.5$, $\mu_r = 0.1$ (moderate compressibility and non-negligible Coulomb and covolume effects). Red (I), blue (T) and dashed-black (R) curves correspond to the associated pressure-velocity curves of the incident, transmitted and reflected shocks, respectively. For convenience, the axes are nondimensionalised with p_0 and c_{0r}, respectively. The red circles are determined by the incident shock intensity, so that $u_1/c_{0r} = (1-\mathcal{R}_i^{-1})\mathcal{M}_i$ and $p_1/p_0 = \mathcal{P}_i$. The blue circles, on the other hand, are given by the equilibrium condition, see (S.1.3) and

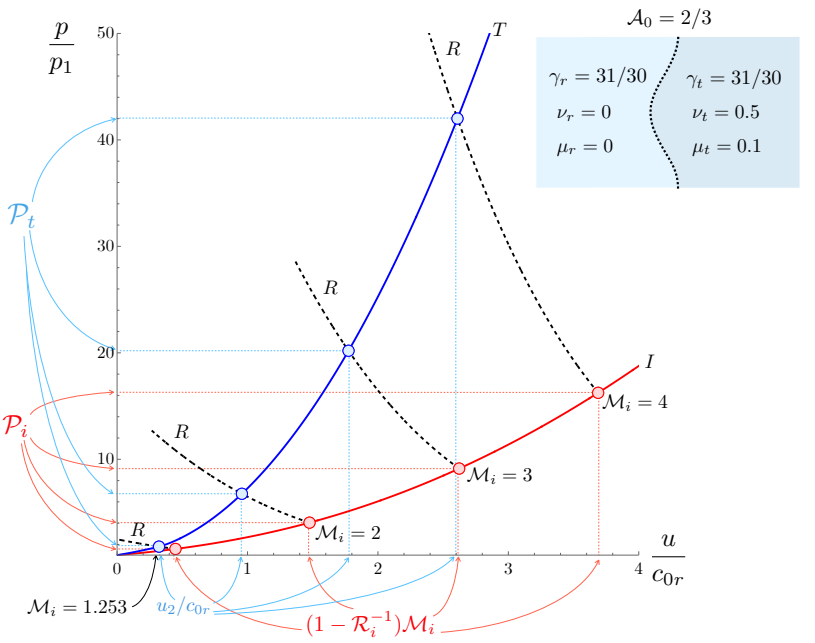

Figure S.1: Solution of the base-flow interaction of a planar shock crossing an interface separating a vdW gas (right side) and an ideal gas (left side). Conditions are computed for $\mathcal{M}_i = 1.253$, as in Fig.2 c) of the main text, and 2, 3, 4. The Atwood number is $\mathcal{A}_0 = 2/3$.

(S.1.4), that finally determines the intensities of the transmitted and reflected shocks, along with the postshock flow properties.

We want to emphasise that the linear theory developed in this study exclusively pertains to the shock-reflected scenario. In order for this condition to hold, it is imperative that the blue curve (T) be positioned above the red curve (I). Consequently, equilibrium, under a specified incident shock intensity, can solely be achieved via compression, i.e., a reflected shock (R). This might not be easy to anticipate when the EoS parameters describing the two fluids are very different. For non-ideal EoS, the type of problem (reflected shock or rarefaction) might be predicted numerically. There exists the possibility of neutral interactions. Such cases refer to conditions where there is no reflected wave (or it takes the form of a simple acoustic wave when the interface is distorted). It occurs when the blue (T) and red (I) curves intersect: $\mathcal{P}_i = \mathcal{P}_t$ and $U_1 = U_2$. For example, within the vdW EoS framework presented in this work, neutral interactions may appear for a large variety of conditions. A general rule is that, for $\gamma_r > \gamma_t$, neutral transmission occurs for positive values of $\mathcal{A}_0$ (the transmitted shock enters in a higher density zone), while the opposite applies for $\gamma_t > \gamma_r$.

In Fig.2 c) of the main text, the evolution of the pressure perturbation at the shocks is illustrated for a case involving two VdW gases under the conditions specified in Fig.S.1, with an incident Mach number of $\mathcal{M}_i = 1.235$. In this scenario, the transmitted shock exhibits Spontaneous Acoustic Emission (SAE), since the parameter h_t exceeds the critical value h_{ct}. Given that this is a very specific case, it is essential to determine whether the SAE condition persists when varying the initial conditions for the same gas configuration, i.e., modifying the incident shock strength and the Atwood number. This analysis is presented in Fig.S.2 as contour plots of the function $h_{ct} - h_t$, where the beige-coloured region indicates SAE or non-decaying oscillations for the transmitted shock in the long-time regime. It is readily seen that such neutrally stable condition is more sensitive to variations in shock strength $\mathcal{M}_i$

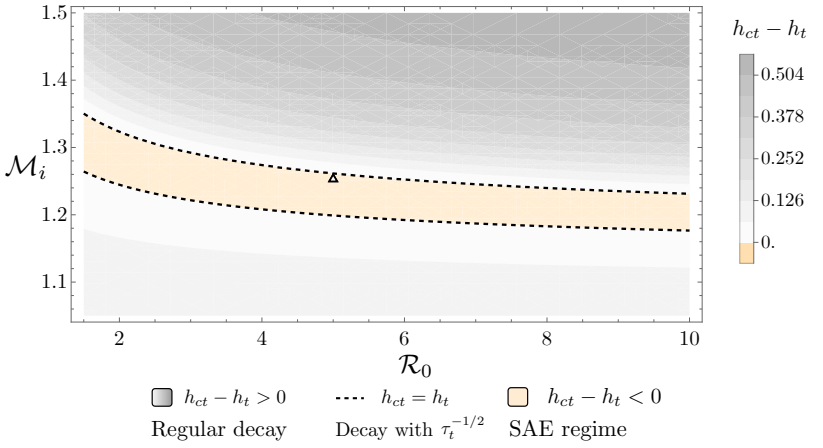

Figure S.2: SAE regime through the function $h_{ct} - h_t$, for varying incident shock strengths and preshock density jump ratios. The gases conditions correspond to those in Fig.S.1

than to changes in the pre-shock density jump $\mathcal{R}_0 = (1 - \mathcal{A}_0)/(1 + \mathcal{A}_0)$. The triangle marker represents conditions in Fig.2 c) of the main text.

S.3. Equilibrium conditions for condensed metals: aluminium and copper

To describe the RMI occurring when a shock crosses a perturbed planar interface separating two condensed materials, the three-term equation of state (EoS) is utilised. This model, consistent with the framework detailed in Chapter XI, § 6, of Zel'dovich & Raizer (2002) and used as an example in Velikovich & Giuliani (2018); Huete *et al.* (2021); Calvo-Rivera *et al.* (2023) in accretion-shock and piston-driven shocks configurations, offers a fairly precise description within pressure ranges extending to several Mbar. The pressure and specific internal energy are delineated as aggregations of three distinct components:

$$p(\rho, T) = p_c(\rho) + p_l(\rho, T) + p_e(\rho, T), \tag{S.3.1}$$

$$E(\rho, T) = E_c(\rho) + E_l(T) + E_e(\rho, T), \tag{S.3.2}$$

where the cold, or elastic, terms, p_c and E_c, are related to the forces of interaction between the atoms of the material at $T = 0$, and therefore they depend only on the material density ρ. The thermal ion (lattice) terms, p_l and E_l, as well as the thermal electron terms, p_e and E_e, are functions of both density and temperature.

For the cold metal, the repulsive forces between atoms due to their interactions do not include thermal energy is present. We use Molodets' analytical approximation (Molodets 1995) for the density dependence of the Grüneisen coefficient

$$\Gamma = \frac{2}{3} + \frac{2\rho_{0a}}{a\rho - \rho_{0a}}, \tag{S.3.3}$$

where ρ_{0a} is the density extrapolated to zero temperature and pressure and a is a dimensionless constitutive parameter that must not be confused with the dimensional parameter in the vdW EoS (S.2.1). With the aid of the Landau–Slater formula (Slater 1955; Landau & Stanyukovich 1945) and the definition of cold energy $p_c = \rho^2 \mathrm{d}E_c/\mathrm{d}\rho$, cold pressure and

internal energies are expressed as explicit functions in the form:

$$p_c(z) = \frac{3K_{0a}}{(a-1)^4}\left(\frac{1}{5}a^4z^{5/3} - 2a^3z^{2/3} - 6a^2z^{-1/3} + az^{-4/3} - \frac{1}{7}z^{-7/3} - \frac{1}{5}a^4 + 2a^3 + 6a^2 - a + \frac{1}{7}\right), \tag{S.3.4}$$

$$E_c(z) = \frac{3K_{0a}}{\rho_{0a}(a-1)^4}\left(\frac{3}{10}a^4z^{2/3} - 6a^3z^{-1/3} + \frac{7a^4 - 70a^3 - 210a^2 + 35a - 5}{35}z^{-1} + \frac{9}{2}a^2z^{-4/3} - \frac{3}{7}az^{-7/3} + \frac{3}{70}z^{-10/3} - \frac{35a^4 + 280a^3 - 105a^2 + 40a - 7}{70}\right), \tag{S.3.5}$$

where K_{0a} is the adiabatic bulk modulus extrapolated to zero temperature and pressure and $z = \rho/\rho_{0a}$ is the normalised density. For the ion lattice (thermal) contributions to the pressure and internal energy, which take into account the vibrations resulting from the changes in the kinetic energy of the ions as the temperature varies, we have

$$p_l(z,T) = \rho_{0a}\frac{3}{m_a}z\Gamma(z)k_BT, \qquad E_l(T) = \frac{3}{m_a}k_BT, \tag{S.3.6}$$

where m_a is the atom mass and k_B is the Boltzmann constant. Finally, the electron contributions are

$$p_e(z,T) = \frac{1}{3}B_0z^{1/3}T^2, \qquad E_e(z,T) = \frac{1}{2}B_0z^{-2/3}T^2, \tag{S.3.7}$$

where B_0 is determined by the number of free electrons per unit mass of the material at $T = 0$ and $\rho = \rho_{0a}$. In deriving (S.3.7), the electronic Grüneisen coefficient has taken to be 2/3, then the density and temperature dependence would exactly correspond to a free electron gas at a temperature well below the Fermi energy.

As done for the VdW EoS, the problem formulation calls for the definition of the sonic coefficient $\kappa = \rho c^2/p$ that take the following form

$$\kappa = \frac{\rho c^2}{p} = \frac{\gamma_c p_c + \gamma_l p_l + \gamma_e p_e}{p_c + p_l + p_e}. \tag{S.3.8}$$

The corresponding values of γ_c, γ_l and γ_e associated with cold, lattice and electronic contributions are, respectively,

$$\gamma_c = \frac{K_{0a}}{p_c}\frac{(az-1)^4}{(a-1)^4z^{10/3}}, \quad \gamma_l = \frac{\mathrm{d}\ln\Gamma}{\mathrm{d}\ln z} + \Gamma + 1, \quad \text{and} \quad \gamma_e = 5/3. \tag{S.3.9}$$

To compute the adiabat curve, the energy conservation equation is conveniently written as

$$H = E_d - E_u - \left(\frac{1}{z_u} - \frac{1}{z_d}\right)\frac{p_d + p_u}{2\rho_{0a}} = 0, \tag{S.3.10}$$

where H is defined as the Hugoniot relationship and the subscripts u and d denote the variables right ahead of (upstream) and behind (downstream) the shock, respectively. The Mach number squared associated with each shock is

$$\mathcal{M}_j^2 = \frac{z_{dj}(p_{dj} - p_{uj})}{z_{uj}(z_{dj} - z_{uj})\rho_{0a}c_{uj}^2}, \tag{S.3.11}$$

where the subscript j may refer to incident (i), transmitted (t), or reflected (r) shock. This

	ρ_{0a} [g/cm^3]	ρ_0 [g/cm^3]	$\Gamma(\rho=\rho_{0a})$	a	K_{0a} [GPa]	B_0 [ergs/gK^2]
Al	2.789414	2.71	1.798175	2.767552	91.133	500
Cu	9.075238	8.93	2.421139	2.139944	146.16	110

Table S.1: Equation-of-state constants for Al and Cu, and parameters according to Molodets (1995) and Al'Tshuler *et al.* (1960a) for aluminium and copper.

relationship can be used to write $\mathcal{R}_j = z_{dj}/z_{uj}$ as a function of the shock strength $\mathcal{M}_j$. Likewise, the postshock Mach number is $\mathcal{M}_{2j} = c_{uj}\mathcal{M}_j/(c_{dj}\mathcal{R}_j)$.

As commented before, along with the base-flow properties, the analysis of the perturbed problem that leads to the RMI demands additional parameters. One of them is the DK parameter that measures the post-shock RH slope, which reads as

$$h_j = -\frac{z_{uj}(p_{dj}-p_{uj})}{z_{dj}(z_{dj}-z_{uj})}\left[\frac{\partial p_{dj}}{\partial z_{dj}} - \frac{\partial p_{dj}}{\partial T_{dj}}\left(\frac{\partial H_j/\partial z_{dj}}{\partial H_j/\partial T_{dj}}\right)\right]^{-1} \tag{S.3.12}$$

that involves the know of the Hugoniot function in (S.3.10).

The system of equations that provide the corresponding mechanical equilibrium at the interface is similar to that described in (S.1.3) and (S.1.4), which can be used to provide the associated dimensionless parameters that govern the linear system. In particular, the values of the initial shocks and interface ripples are given by (S.2.10) and (S.2.11), respectively, and the β parameter that characterises the acoustic coupling is specifically given by (S.2.12).

As in Fig.S.1, the relation between the shock pressure jumps and the fluid particle velocities is provided in Fig.S.3 for a shock wave moving in aluminium and crossing a planar interface separating it from copper material. The scale of pressure jump for $\mathcal{M}_i \leqslant 2.5$ behind the reflected and transmitted shocks approaches the range of the Mbar for materials in preshock in unstressed conditions. We examine the case of RMI in an Al-Cu system, similar to the numerical results presented by Tahir *et al.* (2011) (case II), which also correspond to the cases shown in panels (e) and (f) of Fig.2 in the main text. The incident shock Mach numbers associated with incident shock pressures $p_1 = 0.28$ Mbar and 2.9 Mbar are $\mathcal{M}_i \sim 1.3$ and $\mathcal{M}_i \sim 2.5$, respectively, according to the three-term EoS model. Two other intermediate conditions, $\mathcal{M}_i = 1.5$ and 2, are also computed.

Pre-shock pressure and speed-of-sound conditions are *ad-hoc* provided, namely $p_0 = 1$ bar, $c_{0r} = 6420$ m/s, and $c_{0t} = 4760$ m/s, because the three-term EoS is less accurate in low-pressure conditions. When comparing with Tahir *et al.* (2011) values, we find that the presented EoS model, despite its simplicity, captures the density jumps fairly well. As expected, for weak shocks ($p_1 \sim 0.28$ Mbar), our post-shock density values, $\rho_{2r} = 3.5$ g/cm^3 and $\rho_{2t} = 10$ g/cm^3, slightly over-predict the post-shock values when compared with 3.1 and 9.9 obtained in the numerical simulations. On the other hand, for $p_1 \sim 2.88$ Mbar, we find that $\rho_{2r} = 6.2$ g/cm^3 and $\rho_{2t} = 15.6$ g/cm^3, which compares better with 6.2 and 15.3 in Tahir *et al.* (2011). However, the main advantages of the linear RMI model described in the main text are that it is formulated to accommodate any EoS, so more elaborate models that can provide a better fit for different materials can equally be computed to supply the required values for the linear model

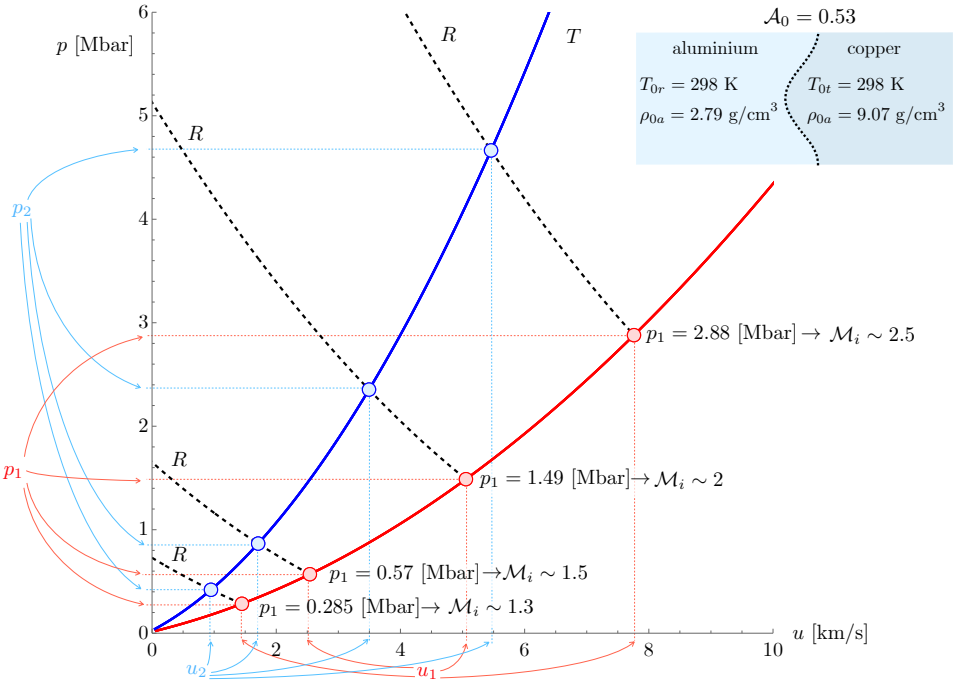

Figure S.3: Solution of the base-flow interaction of a planar shock crossing an interface separating copper (right side) and an aluminium (left side) at room temperature. Equilibrium conditions are shown for incident Mach numbers $\mathcal{M}_i$ = 1.3, 1.5, 2 and 2.5, and for the Atwood number $\mathcal{A}_0$ = 0.53.

REFERENCES

Al'Tshuler, L.V., Kormer, S.B., Bakanova, A.A. & Trunin, R.F. 1960a Equations of state for aluminum, copper and lead in the high pressure region. *Sov. Phys. JETP* **11** (3), 573–579.

Calvo-Rivera, A., Velikovich, A. L. & Huete, C. 2023 On the stability of piston-driven planar shocks. *Journal of Fluid Mechanics* **964**, A33.

Huete, C., Velikovich, A. L., Martínez-Ruiz, D. & Calvo-Rivera, A. 2021 Stability of expanding accretion shocks for an arbitrary equation of state. *Journal of Fluid Mechanics* **927**, A35.

Landau, L.D. & Stanyukovich, K.P. 1945 On a study of the detonation of condensed explosives. *Compt. Rend. (Dokl.) Acad. Sci. URSS* **46**, 362.

Molodets, AM 1995 Generalized Grüneisen function for condensed media. *Combustion, Explosion, and Shock Waves* **31** (5), 620–621.

Slater, J.C. 1955 *Introduction to Chemical Physics*. McGraw-Hill, International Series in Physics.

Tahir, N.A., Shutov, A., Zharkov, A.P., Piriz, A.R. & Stöhlker, Th. 2011 Generation of plane shocks using intense heavy ion beams: Application to Richtmyer–Meshkov instability growth studies. *Physics of Plasmas* **18** (3) 032704.

Velikovich, A.L. & Giuliani, J.L. 2018 Solution of the noh problem with an arbitrary equation of state. *Physical Review E* **98** (1), 013105.

Zel'dovich, Ya. B. & Raizer, Yu P. 2002 *Physics of shock waves and high-temperature hydrodynamic phenomena*. Courier Corporation.